Pre-edge fine structure of the 3d atom K x-ray absorption spectra and quantitative atomic structure determinations for ferroelectric perovskite structure crystals



1998 J. Phys.: Condens. Matter 10 9561

(http://iopscience.iop.org/0953-8984/10/42/021)

J. Phys.: Condens. Matter **10** (1998) 9561–9580. Printed in the UK PII: S0953-8984(98)92803-X

# Pre-edge fine structure of the 3d atom K x-ray absorption spectra and quantitative atomic structure determinations for ferroelectric perovskite structure crystals

R V Vedrinskii, V L Kraizman, A A Novakovich, Ph V Demekhin and S V Urazhdin

Department of Physics, Rostov State University, 5 Zorghe Street, Rostov on Don, 344090, Russia†

Received 24 March 1998, in final form 29 July 1998

**Abstract.** A complete interpretation is proposed for the pre-edge fine structure (PEFS) of the x-ray Ti K-absorption spectra for $ATiO_3$ perovskite structure crystals. The interpretation is based on the results of numerous calculations performed by a modified full multiple scattering method which provides the theoretical spectra for the 3d transition metal oxides in fair agreement with experiment. It is shown that the three main peaks in the PEFS have quite different origin. The first long-wave side peak A is caused mainly by quadrupole transitions. The middle peak B is caused by the p–d mixture effect and the high intensity of it is considered to be a qualitative spectroscopic indication of ferroelectricity in the perovskite structure crystal. A simple formula is obtained which expresses the area under peak B through the lattice constants and mean-square displacement of the absorbing Ti atom from the instantaneous centre of the coordination polyhedron. The peak B area averaged over thermal atomic vibrations is determined by the three-particle atomic distribution function. The short-wave side peak C is caused by the Ti 1s electron transition to the unoccupied 3d states of the neighbouring transition metal atoms. We show that an additional peak C′ on the short-wave side of peak C occurs if there are 4d atoms (for instance Zr atoms in the vicinity of the absorbing Ti atom in the $PbTi_xZr_{1-x}O_3$ (PZT) solid solution) within the oxygen atom octahedrons surrounding the absorbing 3d atom. The area under peak C′ is directly determined by the average number of 4d atoms in the vicinity of the absorbing Ti one.

## 1. Introduction

The progress of x-ray absorption spectroscopy as an element-sensitive method for short-range order atomic structure determinations is mainly associated with extended x-ray absorption fine structure (EXAFS) analysis. The existence of explicit equations expressing the oscillating part of the x-ray absorption cross section (XACS) through the atomic structure parameters has enabled the development of a straightforward method for determining the atomic radial distribution functions. Unfortunately, similar equations cannot be derived in general for the x-ray absorption near-edge structure (XANES) because of the complicated character of the mechanisms of XANES formation. Meanwhile, there are particular but important cases when some XANES features have comparatively clear origin and hence could be used for direct determination of the local atomic structure parameters. We mean more or less prominent features which occur below the main rise of the XACS in the 3d transition metal (TM) K-absorption spectra for some complexes and dielectric crystals [1, 2]. These features which are often called pre-edge fine structure (PEFS) have been shown to be caused

† E-mail address: vedr@iphys.rnd.runnet.ru.

0953-8984/98/429561+20$19.50  

by transitions of the TM 1s electron to the unoccupied electron states near the conduction band (CB) bottom originating mainly from the vacant 3d atomic orbitals (AO) of the TM atoms in the compound. Such transitions are dipole-forbidden for the free atoms but can become dipole-allowed for the TM atoms in the medium. The PEFS is more pronounced in the spectra for TM atoms from the beginning of the 3d row where the number of vacant 3d AO per atom is maximum and decreases towards the end of the 3d row owing to the decrease of the vacant 3d AO number, the decrease of the TM 3d AO overlapping with the neighbouring atom orbitals, and the increase of the many-electron effects. The PEFS often demonstrates sharp polarization and orientational dependence for single crystals with low symmetry environment of TM atoms [3–5]. Moreover, in such crystals the PEFS appears to be most prominent. If TM atoms are disposed in oxygen atom octahedrons as in the perovskite-structure oxides under consideration the intensive pre-edge peaks are an indicator of large static or/and dynamic displacements of the TM atom from the immediate octahedron centre.

The possibility of using PEFS for electron structure studies has been demonstrated in [6–8] where the valence states of iron atoms have been determined in several compounds by PEFS analysis. Atomic structure studies based on PEFS analysis were performed for the first time in [9, 10] where the nature of the ferroelectric phase transition in lead titanate was investigated. It was shown in these papers that the PEFS intensities for the polycrystal $PbTiO_3$ sample are approximately the same for both tetragonal and cubic phases whereas the static displacements of Ti atoms from the inversion symmetry positions in the crystal lattice measured by x-ray or neutron diffraction are as large as 0.3 Å below the Curie point and equal to zero above it. These two facts have enabled the authors [9] to give a preference to the order–disorder model for the phase transition in lead titanate. Such a conclusion has been confirmed by later studies [11]. The contradiction between the results obtained by x-ray absorption spectroscopy and diffraction methods is caused by the well known fact that diffraction methods provide information about the average positions of the atoms in the crystal lattice whereas the x-ray absorption spectrum (XAS) is determined by the average interatomic distances. In other words, Bragg diffraction is determined by the one-particle atomic distribution function whereas XAS is determined by atomic distribution functions of higher orders (for example, in the single scattering approximation, which is sufficient for EXAFS, the spectra are determined by two-particle distribution functions).

The aim of the present paper is to give a complete interpretation of the PEFS for titanium oxides with perovskite structure (including solid solutions) in both paraelectric and ferroelectric phases and to develop a theoretical foundation for the method of quantitative determinations of small displacements of TM atoms from their inversion symmetry positions relative to the instantaneous positions of neighbouring oxygen atoms by PEFS analysis. We will consider only spectra for compounds with Ti atoms in the $3d^0$ state in order to exclude the complications caused by the interaction of 3d electrons in the CB. The well known similarity of general XANES behaviour for different $3d^0$ TM atom oxides [2] is caused by the similarity of the electron structure of these compounds. The wavefunctions of valence bands and of the lowest CBs for these compounds can be reasonably described within the linear combination of atomic orbitals approach as superpositions of TM 3d and O 2p AO [12, 13]. The gap is usually close to 3 eV. The TM atom $L_{2,3}$-spectra in these compounds display sharp and intensive white lines [14, 15] just above the $L_{2,3}$-edge which are obviously caused by dipole-allowed transitions of TM 2p electrons to the unoccupied TM 3d AO. In contrast, due to the absence of the p-symmetry TM atomic-like states near the CB bottom, K-absorption is suppressed in this region and the main rise of XAS only occurs at about 10–15 eV above the K-edge [2]. Nevertheless more or less prominent PEFS peaks appear below the main rise of the TM K-spectra where the CB originated

from the TM 3d AO are disposed. As has been previously proposed, the PEFS can be caused by: (i) the TM 1s electron quadrupole transitions to the unoccupied 3d states of the absorbing TM atom [1, 2]; (ii) the hybridization of p- and d-symmetry states at the absorbing TM atom under the influence of the neighbouring oxygen atoms takes place if the inversion symmetry is broken relative to the absorbing atom instantaneous position [9] (the p–d mixture effect); (iii) the dipole-allowed transitions of the TM 1s-electron into the TM 3d-originated molecular orbitals (MO) of neighbouring octahedrons which are caused by overlapping of these MO with the 1s-wavefunction of the absorbing atom (band effect).

Studies of the mechanisms responsible for PEFS formation and attempts to give an interpretation to PEFS features have been widely performed for crystals with rutile structure where TM atoms are also surrounded by lightly distorted oxygen atom octahedrons: $VO_2$ [16] and $TiO_2$ [17–21, 34]. Nevertheless, the situation is not clear. Theoretical estimations of quadrupole contributions into the Ti K-PEFS [21] contradict experimental studies of quadrupole transition contributions into the PEFS of Ti K-XAS [20, 34]. Interpretations of the peaks in the Ti K-PEFS presented by different authors often contradict each other. In our opinion up until now regular methods have not yet been developed to ascertain unambiguously the nature of these peaks. We propose such methods in the present paper and develop the computational method for quantitative determination of quadrupole contributions into the K-XACS.

Using these methods we study the mechanisms responsible for the PEFS formation in the Ti K-XAS for perovskite-structure titanates. The experimental XANESs [10] for several polycrystal samples (ferroelectric $PbTiO_3$, $BaTiO_3$ and paraelectric $SrTiO_3$, $CaTiO_3$, $EuTiO_3$) are presented in figure 1 where all the spectra are normalized by their high-energy parts. The PEFSs are the fluctuations A, B, C of the absorption coefficients below the main ramp which are disposed of at about 15 eV above the CB bottom. The most intriguing details of these spectra are the peaks labelled B which are significant for the ferroelectric crystals $PbTiO_3$ and $BaTiO_3$ in both tetragonal and cubic phases [9] and are weak for non-ferroelectric crystals such as $SrTiO_3$, $CaTiO_3$, and $EuTiO_3$. It will be shown later that these peaks are caused mainly by the p–d mixture effect and that they can be successfully used for determination of the mean-square displacements of Ti atoms from instantaneous centres of coordination polyhedrons. On the other hand peaks C, which will be shown to be caused by the band effect, can be used for the determination of the average number of 4d-atoms in the third coordination sphere around the absorbing 3d atom in solid solutions with perovskite structure.

We present later the results of thorough calculations of the Ti K-XAS carried out by the modified full multiple scattering method for the tetragonal $PbTiO_3$ monodomain single crystal, the cubic $EuTiO_3$ polycrystal sample and the solid solution $PbTi_xZr_{1-x}O_3$ (PZT) with perovskite structure. Both dipole and quadrupole terms of the photon–electron interaction operator are included in the calculations. The calculation method described in section 2 is based on a new approach to the problems of crystal potential construction and the choice of representative clusters for numerical simulation of the TM K-spectra for oxides. The good overall agreement between the calculated and experimental spectra proves the validity of the calculation method proposed in this paper and enables us to use this method for studies of the mechanisms responsible for PEFS formation. The complete interpretation of all the peaks in the Ti K-XAS PEFS for perovskite-structure titanates is presented in section 3. The formula expressing the peak B area through atomic structure parameters is derived in this section and it is shown that the presence of 4d atoms in the vicinity of the absorbing Ti causes the appearance of the additional peak C′ in the PEFS whose area is directly determined by the number of 4d atoms.

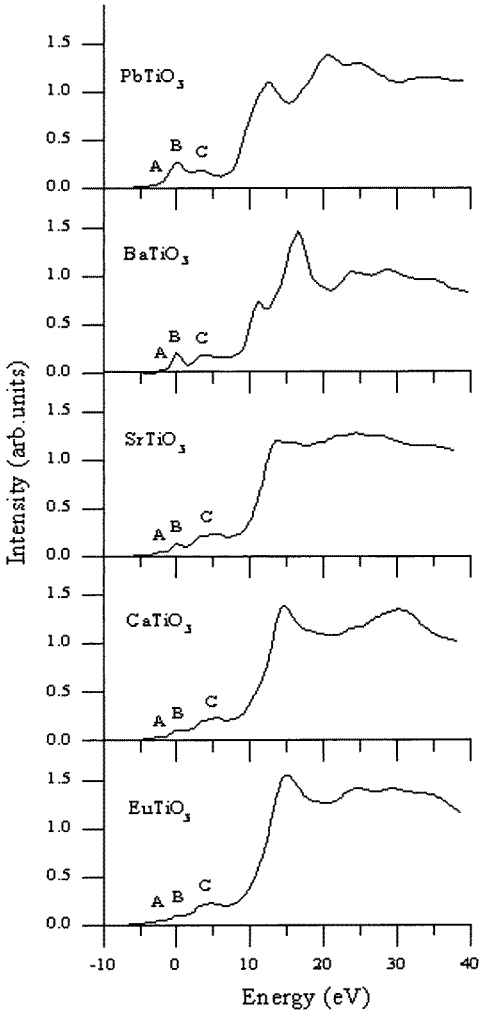


**Figure 1.** Experimental Ti K-XANES [10] for perovskite-structure titanates. All the spectra are matched to each other in the energy scale by the pre-edge peak B.

## 2. Method for calculations

Using one-electron approximation and including the dipole and quadrupole terms of the photon–electron interaction operator one can express the XACS for an atom in a polyatomic system, which will be called hereafter atom number 0, through the photoelectron Green function (GF) $G(\boldsymbol{r}, \boldsymbol{r}', \varepsilon)$ by the equation [22, 24]

$$\sigma_i^0(\omega) = -8\pi\left(\frac{e^2}{hc}\right)h\omega\left[\mathrm{Im}\int \varphi_i^*(\boldsymbol{r})\boldsymbol{e}\boldsymbol{r}G(\boldsymbol{r},\boldsymbol{r}',\varepsilon)\boldsymbol{e}\boldsymbol{r}'\varphi_i(\boldsymbol{r}')\,\mathrm{d}^3 r\,\mathrm{d}^3 r' + \left(\frac{\omega}{2c}\right)^2 \mathrm{Im}\int \varphi_i^*(\boldsymbol{r})\boldsymbol{e}\boldsymbol{r}\cdot\boldsymbol{k}\boldsymbol{r}G(\boldsymbol{r},\boldsymbol{r}',\varepsilon)\boldsymbol{e}\boldsymbol{r}'\cdot\boldsymbol{k}\boldsymbol{r}'\varphi_i(\boldsymbol{r}')\,\mathrm{d}^3 r\,\mathrm{d}^3 r'\right] \quad (1)$$

where $\sigma_i^0(\omega)$ is the cross section of the photo-ionization of the atomic core level $i$ in the isolated atomic sphere number 0 by x-ray waves with frequency $\omega$, $\boldsymbol{e}$ is the electric field vector (polarization vector) of the linear polarized x-ray wave, $\boldsymbol{k}$ is its wavevector, $\varphi_i(\boldsymbol{r})$ is the wavefunction of the atomic level $i$, $\varepsilon$ is the photoelectron energy determined relative to the *muffin-tin* (MT) zero ($E_{MT}$) of the crystal potential.

It is worth noting that in the case of linear polarized x-ray waves under consideration, contrary to the case of circular polarized waves, there is no interference between dipole and quadrupole transition processes and these processes contribute independently to the absorption cross section (1). Thus one is able to calculate these contributions separately.

In order to calculate the GF in the continuum the full multiple scattering method [23–25] which employs MT approximation for the crystal potential is the most suitable. This method is based on the equation which connects the GF $G(\boldsymbol{r}, \boldsymbol{r}', \varepsilon)$ in coordinate representation with the GF matrix $G_{LL'}^{nn'}$ in the so-called 'orbital momentum—number of the atom' representation [24, 25]. We present this equation for the special case when both vectors $\boldsymbol{r}, \boldsymbol{r}'$ are inside the same atomic sphere number 0

$$G(\boldsymbol{r}, \boldsymbol{r}', \varepsilon) = G_0(\boldsymbol{r}, \boldsymbol{r}', \varepsilon) + f \sum_{L,L'} \mathrm{e}^{\mathrm{i}(\delta_l + \delta_{l'})} R_l(\varepsilon, r) Y_L(\hat{\boldsymbol{r}}) G_{LL'}^{00} R_{l'}(\varepsilon, r') Y_{L'}(\hat{\boldsymbol{r}}) \tag{2}$$

where $G_0(\boldsymbol{r}, \boldsymbol{r}', \varepsilon)$ is the GF for the isolated atomic sphere number 0, $Y_L(\hat{\boldsymbol{r}})$ is the real spherical harmonic, $L = (l, m)$, $\hat{\boldsymbol{r}}$ is a unit vector directed along the vector $\boldsymbol{r}$, $\delta_l$ is the partial scattering phase shift for the electron wave with orbital moment $l$ scattered by the zeroth atomic sphere, $f$ is a coefficient ($f = (2m/h^2)^{3/2}(\varepsilon)^{1/2}$) and $R_l(\varepsilon, r)$ is a regular solution of the radial Schrödinger equation for an electron with orbital moment $l$ and energy $\varepsilon$ in the atomic sphere number 0. The solution $R_l(\varepsilon, r)$ is normalized on the surface of the atomic sphere by the following boundary condition

$$R_l(\varepsilon, r_0) = j_l(kr_0)\cos\delta_l - n_l(kr_0)\sin\delta_l \tag{3}$$

where $r_0$ is the radius of the atomic sphere 0, $k$ is the electron wavenumber and $j_l$ and $n_l$ are the spherical Bessel and Neuman functions.

Substituting (2) into (1) one can easily express the XACS through the GF matrix $G_{LL'}^{00}$. For instance, the expression for the K-XACS obtained within the dipole approximation is the following

$$\sigma_K^0(\omega) = 8\pi h\omega \left(\frac{e^2}{hc}\right)\left(\frac{2m}{h^2}\right)^{3/2}\sqrt{\varepsilon}\left|\int \varphi_{1s}(r) r^3 R_1(\varepsilon, r)\,\mathrm{d}r\right|^2 \times \sum_{i,j=1}^{3} e_i e_j \,\mathrm{Im} \sum_{m,m'=-1}^{1} (\mathrm{i}\delta_{mm'} - G_{mm'}^{00}\,\mathrm{e}^{2\mathrm{i}\delta_1}) S_{mi} S_{m'j} \tag{4}$$

where $S_{mi} = \int Y_{1m}(\hat{\boldsymbol{r}})\hat{\boldsymbol{r}}_i Y_{00}(\hat{\boldsymbol{r}})\,\mathrm{d}^2\hat{\boldsymbol{r}}$.

For calculating the GF matrix $G_{LL'}^{n0}$ the following system of linear algebraic equations should be solved [24, 25]

$$G_{LL'}^{n0} = g_{LL'}^{n0} + \sum_{n',L''} g_{LL''}^{nn'} \cdot t_{l''}^{n'} \cdot G_{L''L'}^{n'0} \tag{5}$$

where $t_{l''}^{n'}$ is the partial scattering $t$-matrix for the $n'$th atom in the crystal and the electron orbital momentum $l''$ and $g_{LL''}^{nn'}$ is the coefficient in bicentral expansion for the free electron GF [23].

The core-hole influence on the absorbing atom potential breaks the translational symmetry of the crystal potential and system (5) can be solved if one employs a cluster approximation for the crystal and also restricts the number of orbital moments included in

summation (5). For calculating the XACS in the near-edge region we have included $l \leqslant 3$ for heavy atoms (Pb, Ba, Zr) and $l \leqslant 2$ for others. The correct choice of representative cluster is an important element of the full multiple scattering method and will be discussed later. To include the finite lifetime of the electron–hole pair appearing at the final stage of the photo-ionization process we have smeared the spectra taking into account that the photoelectron lifetime in the medium rapidly decreases with an increase of the photoelectron energy $\varepsilon$.

### *2.1. The cluster potential construction*

Self-consistent calculations of a cluster potential lead to the well known 'cluster effect' which causes the potential of the central atom of the cluster to be more attractive than the potentials of the equivalent atoms which are disposed in the cluster periphery. In order to exclude this effect we approve a semi-empirical approach to the cluster potential construction assuming that the most important point for the XANES calculations is keeping the correct values of the relative energies of the atomic valence levels and/or atomic scattering resonances for different atoms in the crystal. Thus, the potential inside an atomic sphere is considered to be a sum of free atom self-consistent potentials and a constant value (potential shift) simulating both the Maudelung potential and the change of the potential caused by redistribution of the electron density inside the atomic sphere. To estimate the potential shifts we have compared the energies of the atomic levels with those determined by the self-consistent method of augmented plane waves [26]. The shifts obtained in the case considered appear to be so small that it is possible to neglect them. The extended continuum model [27] for the MT potential is employed, i.e. the potential outside the cluster is considered to be equal to the average interstitial potential (MT-zero). This means that we ignore the reflection of the electron waves from the atoms outside the chosen cluster.

The electron density inside each atomic sphere is considered to be equal to that for the corresponding free atom obtained by the usual Herman–Skillman procedure [28] with the exchange parameter $\alpha$ taken according to the Schwarz prescription [29] ($\alpha \approx 0.75$). At the same time the potentials used for $t$-matrix calculations for the vacant electron states in the continuum are determined using a $\alpha$ value which is lower ($\alpha \approx 0.5$–$0.6$) in comparison with the Schwarz one [30]. The reason is that Schwarz chooses $\alpha$ in order to fit the occupied state ionization energies to Hartree–Fock ones, consequently the $X_\alpha$ potential for occupied electron states really includes two terms: the first one simulates the exchange potential and the second cancels the ionized electron self-interaction. Of course, the second term should be excluded for calculating the vacant electron state wavefunctions in the continuum. To do this in a simple way we propose to decrease $\alpha$.

The electron configurations for all atoms in the cluster excluding the absorbing one are chosen to coincide with those for neutral free atoms in the ground state. The configuration of the absorbing atom has been chosen to include extra atomic screening of the core hole. In the case of metals or covalence crystals complete extra atomic screening leads to an increase of the valence shell occupation by one electron. In the case of the ion-covalent crystals under consideration the screening charge should be slightly less than the whole electron charge and we consider it to be an adjustment parameter. As will be shown later the best agreement with experimental Ti K-XANES in the case of $ATiO_3$ crystals is achieved if one increases the 3d-shell occupation of the ionized Ti atom by 0.8 electrons. This result seems to be quite reasonable. The model of the core-hole potential described above will be called hereafter the model of incomplete extra atomic screening. Of course, one should understand that this model cannot be justified rigorously. We use it for simple simulation of

the complicated dynamic processes which take place during x-ray absorption. Nevertheless our studies have shown that the model proposed enables us to calculate with good agreement the experimental TM K-XANESs for various TM oxides [34–36].

### *2.2. The choice of representative cluster*

As was mentioned in the introduction, PEFS is caused by Ti 1s electron transitions to unoccupied electron states originated from Ti 3d AO. These states form two sets of conduction bands in perovskites: lower $t_{2g}$ bands and upper $e_g$ ones. Bands of the first type are caused by $\pi$-type interaction and therefore are more narrow than ones of the second type which are caused by $\sigma$-type interaction [13]. The core-hole potential strongly influences both $e_g$ and $t_{2g}$ MO localized at the $TiO_6$ octahedron containing the ionized Ti atom but the influence of this potential on similar MO localized at the neighbouring octahedrons is weak. To demonstrate the core-hole effect which takes place in the potential model proposed in the previous section we have calculated the d-local density of states (LDOS) of the Ti atom in the ground state (figure 2, curve 1) and the d-LDOS of the Ti atom containing the screened 1s hole (figure 2, curve 2). Both calculations have been performed for the ideal octahedral $TiO_6$ cluster. The Ti–O separation in the cluster equal to 2.0 Å has been employed which approximately corresponds to Ti–O bond lengths in the $ATiO_3$ crystals under consideration. The coordinate axes have been directed along the four-fold symmetry axes of the clusters. One can see from figure 2 that the core-hole potential shifts down both $t_{2g}$ and $e_g$ MO by about 3 eV.

We present also in figure 2 the Ti K spectra calculated for the ideal octahedral $TiO_6$ cluster (curve 3) and for the distorted model $TiO_6'$ cluster with the Ti atom displaced from the centre of the cluster by 0.3 Å along the $z$-axis as occurs in the $PbTiO_3$ crystal in the tetragonal phase. The calculations have been performed for the x-ray polarization vector parallel to the $z$-axis (curve 4) and perpendicular to it (curve 5). All the Ti K-spectra have been calculated for the excited Ti atom employing the same potential as for curve 2. One can see that there is a dramatic difference between the Ti K-spectra for the ideal octahedral $TiO_6$ cluster and for the $TiO_6'$ cluster with the displaced Ti atom. In the first case there is no PEFS whereas in the second case a significant pre-edge peak B appears for the x-ray polarization vector $\boldsymbol{e}$ parallel to the $z$-axis and a minor feature A appears for $\boldsymbol{e} \perp z$. Comparison of the Ti K-spectra (curves 4, 5) with the d-LDOS calculated for the excited Ti atom (curve 2) allows us to easily explain the appearance of such peaks by the p–d mixture effect which is caused by the lack of inversion symmetry for the $TiO_6'$ cluster. We see that the p–d mixture effect is strong in the cluster under consideration for high-energy $e_g$-type MO whereas it is weak for low-energy $t_{2g}$-type ones. Taking into account symmetry considerations it is easy to understand why peak B appears for $\boldsymbol{e} \parallel z$ whereas peak A appears for $\boldsymbol{e} \perp z$.

One notes that the Ti K-XAS PEFS for the $TiO_6'$ cluster does not exhibit the peak C caused by the band effect. Consequently this cluster is not representative for PEFS calculations for the $ATiO_3$ perovskite-structure crystals. The simplest representative cluster of these crystals which is shown in figure 3 contains 51 atoms. This cluster includes, besides the absorbing Ti atom, six nearby Ti atoms each surrounded by six oxygen atoms. Consequently in the vicinity of the absorbing Ti atom in this cluster there are six complete $TiO_6$ octahedrons. Eight A atoms being nearest to the absorbing Ti atom are also included in the cluster. Our calculations have shown that by using such a cluster one is able to obtain the theoretical Ti K-XAS in reasonable agreement with the experimental one in the near-edge region. The enlarging of such a cluster does not change practically the PEFS

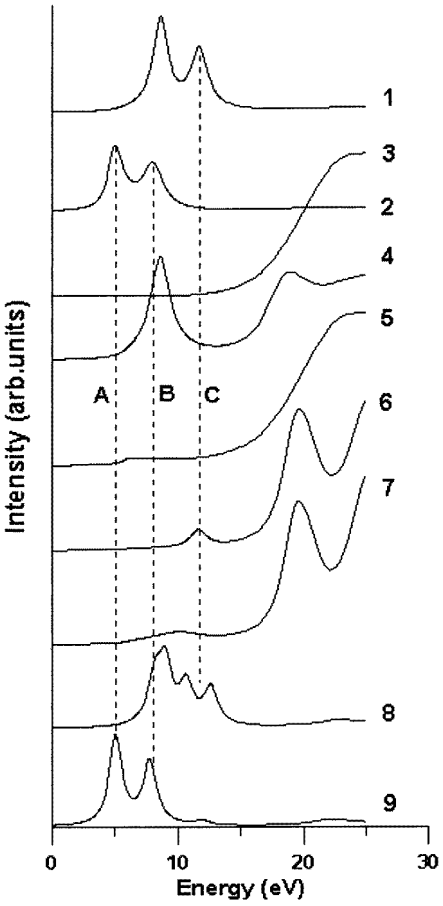


**Figure 2.** The Ti d-LDOS and Ti K-XANES calculated for model clusters. Curves 1 and 2 show the Ti d-LDOS for the ideal octahedric $TiO_6$ cluster in the ground state (1) and in the excited state containing the Ti atom with the screened 1s-hole (2). Curve 3 shows the Ti K-XANES for the same ground-state cluster. Curves 4 and 5 show the Ti K-XANES for the $TiO_6'$ cluster in the excited state with the Ti atom displaced from the centre of the cluster by 0.3 Å along the $z$-axis (curve 4, $\boldsymbol{e} \parallel z$ and curve 5, $\boldsymbol{e} \perp z$). Curves 6 and 7 show the Ti K-XANES for the ideal cubic 51-atomic cluster (6) in the excited state and for the 45-atomic cluster in which the most remote oxygen atoms are absent (7). Curves 8 and 9 show the Ti d-LDOS for the ideal cubic 51-atomic cluster in the ground state (8) and in the excited state (9).

but slightly improves agreement between the theoretical and experimental spectra above the main rise of Ti K-XAS. It is worth noting that in order to perform correct calculations of the pre-edge peak C, clusters containing complete $TiO_6$ octahedrons in the nearest vicinity of the absorbing Ti atom should be used because even the lack of one oxygen atom in each of these octahedrons leads to strong reconstructions of their 3d-originated MO. To illustrate this fact we present in figure 2 the Ti K-XANESs calculated for the mentioned 51-atomic cluster of the ideal cubic $PbTiO_3$ crystal (curve 6) and for the 45-atomic cluster obtained from the 51-atomic cluster by removal of six oxygen atoms which are most remote from the absorbing Ti atom (curve 7). The calculations were performed for the Ti atom containing the screened 1s-hole. We see that the spectrum calculated for the centrally-

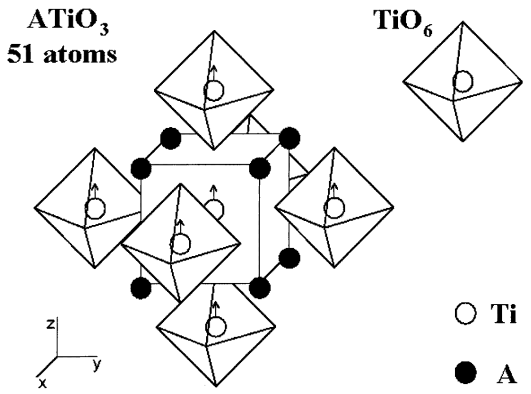


**Figure 3.** The minimum representative cluster of the $ATiO_3$ perovskite-structure crystal.

symmetric 51-atomic cluster does not contain the pre-edge peak caused by the p–d mixture but contains a new peak whose energy is close to that of the $e_g$-MO for the ground-state $TiO_6$ cluster. As follows from curve 7 this peak is dramatically affected by distortion of neighbouring octahedrons to the absorbing Ti atom. Therefore one should conclude that the representative cluster of the $ATiO_3$ crystal must contain only complete $TiO_6$ octahedrons in the nearest vicinity of the absorbing atom if one intends to carry out correct simulation of the PEFS. This important fact has not been taken into account in the papers devoted to cluster simulation of the TM K-PEFS (see for instance [21]).

In order to understand the effects of cluster increase on the d-LDOS at the central Ti atom we have calculated them for the 51-atomic clusters of the ideal cubic $PbTiO_3$ crystal. The results obtained are also presented in figure 2. Curve 8 represents the d-LDOS for the ground-state Ti atom and curve 9 represents that for the Ti atom containing the screened core-hole. One can see that $e_g$ and $t_{2g}$ MO for the $TiO_6$ cluster are split in the case of the extended ground-state cluster. Such splitting is the first step to the formation of $e_g$ and $t_{2g}$ bands of the crystal. As follows from curve 9 the screened core-hole potential shifts down by about 3 eV the energies of both $e_g$ and $t_{2g}$ MO of the central octahedron and thus practically cancels their hybridization with the corresponding MO of neighbouring octahedrons. As a result only two narrow intensive peaks appear in the d-LDOS for the excited Ti atom even in the case of the 51-atomic cluster. This result proves that the band calculations cannot provide either TM L-XANESs or corresponding PEFSs in reasonable agreement with experiment. In order to succeed one must include the core-hole potential. This result is in agreement with that obtained in many papers (see for instance [17]).

## 3. Results and discussion

The main purpose of the present paper is to ascertain the nature of all the peaks in Ti K-XAS PEFSs for perovskite-structure oxides. To solve this problem we have thoroughly studied the dependence of theoretical PEFSs on cluster size, the positions of atoms in the clusters, the direction of the x-ray polarization vector $\boldsymbol{e}$ and atomic potentials etc. Of course, before starting such studies it is necessary to first prove that the method used for the calculations provides theoretical spectra in good agreement with experiment. To do this we have calculated and compared with the experimental data presented in [10, 33, 37] Ti K-XANESs for the tetragonal $PbTiO_3$ monodomain single crystal measured for different

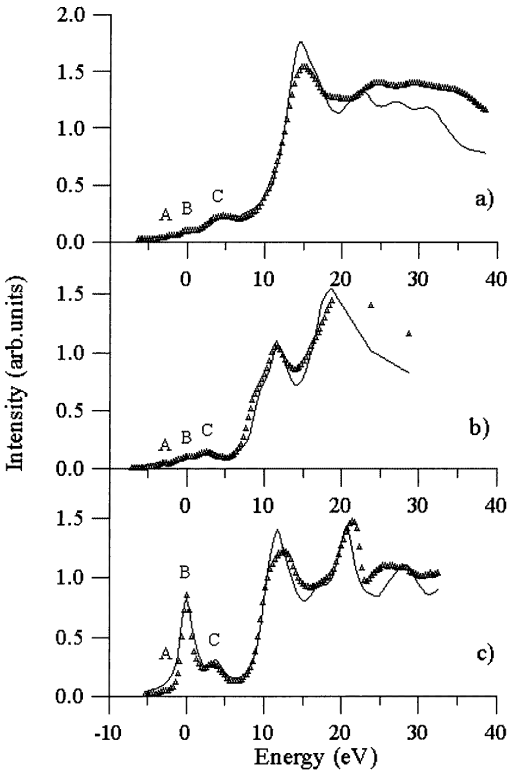


**Figure 4.** Comparison of the theoretical (full curves) and experimental [10, 37] (triangles) Ti K-XANES for: the $EuTiO_3$ polycrystal sample (a), and the $PbTiO_3$ monodomain single crystal (b) $\boldsymbol{e} \perp z$ and (c) $\boldsymbol{e} \parallel z$.

directions of the x-ray polarization vector and for the cubic $EuTiO_3$ polycrystal sample. The calculations have been performed for the 199-atomic clusters. Both dipole and quadrupole terms of the electron–photon interaction operator have been included. To begin we have not taken into account atomic vibrations and have considered that all atoms are exactly placed into the lattice sites determined by diffraction methods at room temperature [31, 32]. The calculated spectra for the $PbTiO_3$ single crystal appear to be in fair overall agreement with experiment as can be seen from figures 4(b) and (c) where theoretical (full curves) and experimental [37] (triangles) spectra obtained for different directions of the x-ray polarization vector $\boldsymbol{e}$ are presented. In contrast, peak B in the calculated PEFS for $EuTiO_3$ appears to be too weak in comparison with experiment [10]. The most probable reason for this discrepancy is the influence of atomic thermal vibrations on the experimental spectra which provide a dipole contribution to the peak B caused by the p–d-mixture effect. To simulate the influence of the atom vibrations on the PEFS we calculate the Ti K-XANES for the absorbing Ti atom being displaced from the inversion symmetry position in the $EuTiO_3$ lattice by 0.08 Å which is a reasonable value for the atom vibration amplitude. In order to compare the calculated spectra with the experimental ones which were measured for the polycrystal sample we have calculated the spectra for different orientations of $\boldsymbol{e}$ and $\boldsymbol{k}$ vectors and have averaged the spectra obtained. The results of such calculations, which are presented in figure 4(a) (full curve), demonstrate good

overall agreement with the experiment [10] (triangles) in the near-edge region. In order to perform a more thorough comparison of theory and experiment we have decomposed the theoretical and experimental PEFSs for the $EuTiO_3$ polycrystal sample into distinct peaks assuming each of them has Voight function form. The results of decomposition are shown in figure 5 where the dotted curves show the components of the experimental spectrum and the dashed curves show the components of the calculated spectrum. Comparison of theoretical and experimental spectra performed in figures 4 and 5 demonstrate that the method for calculations proposed in section 2 enables one to calculate the Ti K-XAS PEFSs for the perovskites in fair agreement with experiment. Such agreement proves this method to be sufficient for studies of the mechanisms of PEFS formation in perovskite-structure crystals.

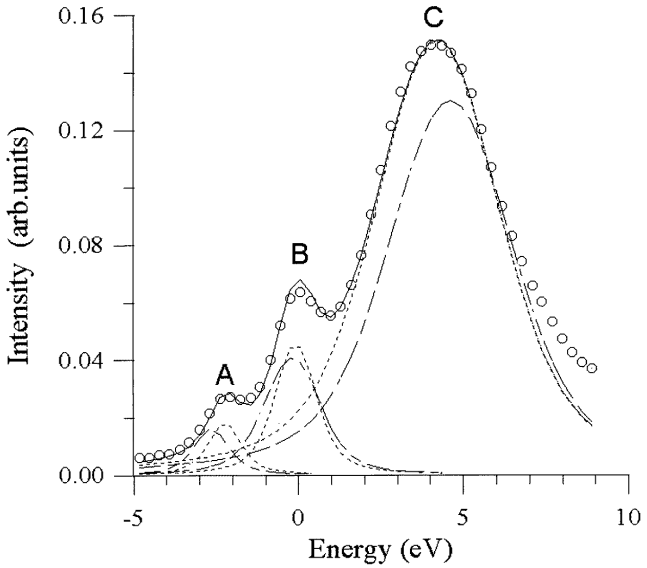


**Figure 5.** Comparison of the pre-edge peaks obtained by decomposition of the theoretical and experimental [10] Ti K-XANES for the $EuTiO_3$ polycrystal sample. The experimental peaks are shown by the dotted curves whereas the theoretical peaks are shown by the dashed curves.

### *3.1. Interpretation of the PEFS peaks*

In order to ascertain the nature of different peaks in the TM K-XAS PEFS for a non-cubic crystal it is reasonable to answer several questions: (i) whether the TM 3d-shell can be considered approximately split by the nearest environment to two subshells of the $e_g$ and $t_{2g}$ types or whether splitting is more complicated; and (ii) which peaks in the PEFS are caused by TM 1s-electron transitions to the 3d-originated MO localized at the absorbing TM atom and which ones are caused by transitions to MO localized at the neighbouring TM atoms. To answer these questions for $ATiO_3$ perovskite-structure oxides we have performed numerous calculations for the 7-atomic $TiO_6$ and 51-atomic clusters of the tetragonal $PbTiO_3$ crystal, which is the most distorted among the perovskites considered. Since the final states of the quadrupole transitions are quite evident we consider in this section mainly the dipole contributions to the spectra. For (i) we have calculated the Ti d-LDOS for both ground and excited states of the central Ti atom in the clusters used. The results obtained are shown

in figure 6, curves 1–4. Comparing them with those presented in figure 2 (curves 1, 2, 8, and 9) which were calculated for similar clusters but with cubic symmetry one can see that the tetragonal distortion even in the case of the $PbTiO_3$ crystal does not cause visible reconstruction of the Ti d-LDOS. This result permits one to use the notations $e_g$ and $t_{2g}$ for the maxima in the Ti d-LDOS for all $ATiO_3$ crystals.

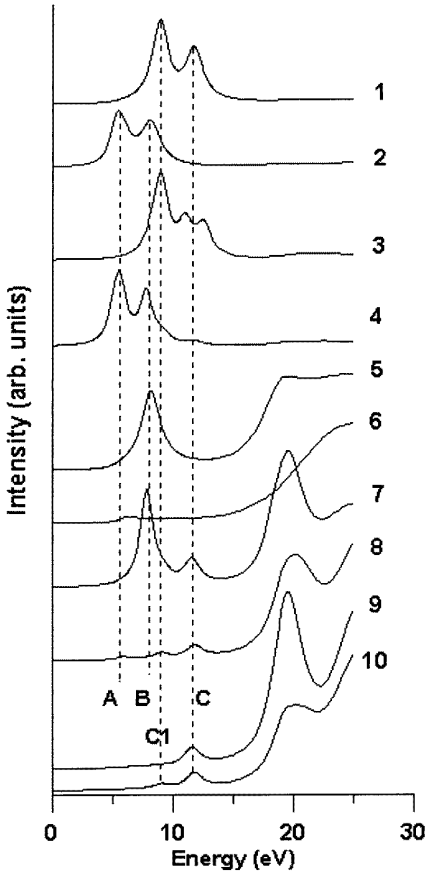


**Figure 6.** The Ti d-LDOS and Ti K-XANES calculated for the clusters of the tetragonal $PbTiO_3$ crystal. Curves 1 and 2 show the d-LDOS for the ground-state $TiO_6$ cluster (1) and the excited-state one (2). Curves 3 and 4 show the same LDOS obtained for the 51-atomic cluster. Curves 5 and 6 show the Ti K-XANES calculated for the excited-state $TiO_6$ cluster (curve 5, $\boldsymbol{e} \parallel z$ and curve 6, $\boldsymbol{e} \perp z$). Curves 7 and 8 show the Ti K-XANES calculated for the excited-state 51-atomic cluster (curve 7, $\boldsymbol{e} \parallel z$ and curve 8, $\boldsymbol{e} \perp z$). Curves 9 and 10 show similar spectra calculated for the model cluster of the tetragonal crystal with the absorbing Ti atom placed exactly into the centre of its coordination polyhedron.

The results of the calculations performed for the representative 51-atomic cluster of the tetragonal $PbTiO_3$ crystal are shown in figure 6, curves 7 ($\boldsymbol{e} \parallel z$) and 8 ($\boldsymbol{e} \perp z$) where $z$ is the four-fold axis. We have considered the atoms in the cluster to be placed exactly into the lattice sites determined by diffraction methods [31, 32] at room temperature. According to the prescriptions of section 2.1 we have used the following electron configuration for the absorbing Ti atom: $1s^1 \ldots 3d^{2.8}4s^2$. We see that for $\boldsymbol{e} \parallel z$ there are two peaks in the PEFS: the very intensive peak B and rather weak peak C. The position of peak B is close to the $e_g$

maximum in the d-LDOS for the excited Ti atom whereas peak C energy is close to that of the $e_g$ maximum in the d-LDOS for the ground state Ti atom. In contrast, there are three peaks in the PEFS for $\boldsymbol{e} \perp z$: the very weak peak A whose energy nearly coincides with that of the $t_{2g}$ maximum in the d-LDOS for the excited Ti atom; peak C whose area and position are close to the corresponding parameters of the peak C for $\boldsymbol{e} \parallel z$; and peak C1 whose energy is close to that of the $t_{2g}$ maximum in the d-LDOS for the ground state Ti atom. As was proposed in section 2.2 peaks A and B, which appear even in the case of the 7-atomic $TiO_6$ clusters with broken inversion symmetry (see figure 6, curves 5 and 6 and figure 2, curves 4 and 5), are caused by the p–d mixture effect whereas peak C is caused by the band effect. To prove this assumption and to ascertain the nature of the C1 peak which does not appear for the model clusters employed in section 2.2 we have performed the following computer experiments. First, we show that a change of the central Ti atom potential causes a similar change of energies of peaks A and B whereas the positions of peaks C and C1 do not change at all. In contrast, a change of the potentials of environmental Ti atoms causes a similar change of energies of peaks C and C1 without any change in the positions of peaks A and B. Taking into account that the Ti 3d-states are the only atomic-like states near the CB bottom one can conclude from these results that the wavefunctions of the A and B resonances contain large contributions of the absorbing Ti atom 3d-AO whereas the wavefunctions of the C and C1 resonances contain large contributions of the neighbouring Ti atom 3d-AO. Second, we calculate the Ti K-XANES for a model 51-atomic cluster of the tetragonal $PbTiO_3$ crystal with the central Ti atom placed exactly into the centre of its coordination polyhedron but without any changes in the positions of the environmental Ti atoms. The calculated spectra are shown in figure 6, curves 9 ($\boldsymbol{e} \parallel z$) and 10 ($\boldsymbol{e} \perp z$). One can see that peaks A and B are absent in these spectra whereas peaks C and C1 are nearly the same as in curves 7 and 8. Therefore, the results of the computer experiment unambiguously confirm the interpretation of the peaks in the PEFS proposed in section 2.2 and show that the peak C1 is caused by the band effect as well as peak C.

It is worth noting that according to these results both p–d mixture and band effects can provide intensive PEFS peaks caused by transitions to $e_g$-type MO but all the peaks caused by transitions to the $t_{2g}$-type MO for perovskite-structure crystals are very weak. The reason that peak A is very weak is not trivial and it will be considered elsewhere. In contrast, it is easy to explain the weakness of the peak C1. The reason is that for cubic perovskite-structure crystals this peak is absent (see curve 6, figure 2) because the $t_{2g}$ MO of neighbouring $TiO_6$ octahedrons do not overlap with the Ti 1s-orbital of the central absorbing Ti atom. The weak C1 peak appears only in the case of the tetragonally distorted crystal for $\boldsymbol{e} \perp z$. This result is in agreement with experiment. Really thorough processing of the Ti K-PEFS for the tetragonal $PbTiO_3$ single crystal measured for $\boldsymbol{e} \perp z$ demonstrates the existence of the weak peak C1 slightly above peak B which is also weak in such a case (see figure 4, curve 3). Of course, the C1 peak is weak for all the perovskite-structure crystals but the situation can be quite different for the crystals with different character of the $TiO_6$ octahedron linkage. For instance, the most intensive middle peak in the Ti K-PEFS for the $TiO_2$ rutile crystal is caused, according to the interpretation proposed in [18–20], mainly by the same mechanism as the C1 peak for the perovskites, i.e. by transitions to the $t_{2g}$ conduction band of the crystal. (The authors of paper [21] consider this mechanism to be responsible for the appearance of the first very weak peak in the PEFS. Such an interpretation contradicts the results of the experimental studies performed in [20, 34] which convincingly prove that the peak mentioned contains a large quadrupole contribution and consequently is caused by transitions to the 3d-originated MO localized at the absorbing Ti atom which are shifted by the core-hole potential relative to the $t_{2g}$ conduction band.)

Of course, the weak peak A is caused not only by the p–d mixture effect but also by quadrupole transitions to the $t_{2g}$-type MO localized at the absorbing Ti atom. Our calculations (see figure 5) have shown that the contribution into peak A from the quadrupole transitions is of the same order as that from the p–d mixture effect.

It is worth noting that the separation between peaks B and C strongly depends on the potential of the ionized Ti atom. The assumption of a completely screened 1s hole (which is close to the often used $(Z+1)$ approximation) according to which the 3d-shell occupation is increased by one electron ($1s^1 \ldots 3d^3 4s^2$ configuration of the ionized Ti atom) results in too small a separation between peaks B and C [35]. In the present paper we employ the model of incomplete extra atomic screening mentioned in section 2.1 according to which the 3d-shell occupation is increased by 0.8 electrons ($1s^1 \ldots 3d^{2.8} 4s^2$ configuration of the ionized Ti atom). Using this model we have obtained the theoretical Ti K-spectra for the $PbTiO_3$ monocrystal in fair agreement with experimental ones (see figures 4(b) and (c)). Of course, it is necessary to stress once more that an increase of the Ti 3d-AO occupation number by 0.8 is a semi-empirical simulation of the complicated dynamic process of rearrangement of valence bands during x-ray absorption. Nevertheless, it has appeared that the model of incomplete extra atomic screening is really suitable for the ionic-covalence $ATiO_3$ crystals and for other TM oxides as is shown by the comparison of our calculations carried out for a number of different TM oxide spectra with experiment (see, for example, [34, 35]).

### *3.2. The dependence of the PEFS intensity on the atomic structure parameters for $ATiO_3$ perovskites*

The PEFS was first employed for the studies of crystal atomic structure in [9] where the nature of the ferroelectric phase transition in lead titanate was investigated. Analysing the temperature dependence of the Ti K-PEFS intensity measured for a polycrystal sample, the authors of [9] arrived at a qualitative conclusion about strong tetragonal dynamic distortions of $TiO_6$ polyhedrons in the high-temperature cubic phase of the $PbTiO_3$ crystal. This result was considered in [9] to confirm an order–disorder model of the ferroelectric phase transition in this crystal.

In order to use the PEFS for quantitative investigations one should at first derive an equation which connects the PEFS intensity with the atomic structure parameters. Such an equation was briefly considered in [11]. In the present paper we will study the problem more thoroughly. As has been shown, the dipole induced peak B in the Ti K-XAS PEFS for perovskites is the most sensitive to displacements of the absorbing atoms from the centrally-symmetric position relative to neighbouring atoms. To derive an equation which connects the peak B area with the atomic structure parameters we have numerically studied the dependence of this area on the positions of the atoms in the 51-atomic $PbTiO_3$ cluster. Of course, such a study should be performed for different directions of the x-ray polarization vector and the results obtained should be averaged over thermal vibrations of the atoms about the sites in both tetragonal and cubic crystals. To simplify the complicated problem, one notes that the experimental x-ray absorption coefficient and, respectively, the peak B area $I_B$, after averaging over atomic thermal vibrations, are the macroscopic characteristics of a crystal and hence should have the same symmetry properties. Consequently, the averaged area $\langle I_B \rangle$ of the dipole induced peak B should not depend on the x-ray polarization vector direction for cubic crystals and should depend on this direction for the tetragonal crystals in the following manner

$$\langle I_B \rangle = I_{\parallel} \cos^2 \theta + I_{\perp} \sin^2 \theta \tag{6}$$

where $\theta$ is the angle between the x-ray polarization vector $\boldsymbol{e}$ and the four-fold $z$ axis of the crystal, $I_{\parallel}$ is the averaged peak B area for $\boldsymbol{e} \parallel z$, and $I_{\perp}$ is that for $\boldsymbol{e} \perp z$ (i.e. for $\boldsymbol{e} \parallel x$ or $y$).

Thus, it is sufficient for our purpose to carry out numerical studies only for two directions of the x-ray polarization vector for the tetragonal crystal (i.e. for $\boldsymbol{e} \parallel z$ and $\boldsymbol{e} \parallel x$) and only for one direction (i.e. for $\boldsymbol{e} \parallel z$) for the cubic crystal. Numerous calculations carried out for various positions of the atoms in the 51-atomic cluster have demonstrated that in both tetragonal and cubic cases the peak B area for $\boldsymbol{e}$ parallel to either $z$ or $x$ crystal axes is determined predominantly by the spacings between only three atoms: the absorbing Ti atom and the two nearest oxygen atoms $O_1$ and $O_2$ disposed together with the Ti atom in the same Ti–O–Ti–O–Ti chain which is parallel to the vector $\boldsymbol{e}$. The analytical expression which fits the calculated peak B area is

$$I_B = K\frac{[u(\mathrm{Ti}) - 0.5(u(\mathrm{O}_1) + u(\mathrm{O}_2))]^2}{[u(\mathrm{O}_1) - u(\mathrm{O}_2)]^{5.5}} \tag{7}$$

where $u$ is the $z$ coordinate of an atom for $\boldsymbol{e} \parallel z$ and is the $x$ (or $y$) coordinate for $\boldsymbol{e} \parallel x$ (or $y$), $K$ is a coefficient which depends neither on the atom displacements nor on the direction of the vector $\boldsymbol{e}$. The numerical studies have shown that the last formula is valid within 10% accuracy up to the displacement values of about 0.3 Å.

The last equation is very encouraging because it demonstrates that even in the near-edge region of the x-ray absorption spectrum there is a peak whose area is simply determined by a small number of atomic structure parameters. Nevertheless the problem of $I_B$ averaging over atomic thermal vibrations and/or structural disorder is complicated enough. Simple equations for the averaged value $\langle I_B \rangle$ can be obtained in two extreme cases.

The first of them takes place if one can assume that variations of the spacing between the $O_1$ and $O_2$ atoms caused by atomic vibrations are relatively small and that this spacing is always close to the corresponding lattice parameter. Within such an approximation the following equation for the averaged area of peak B for the tetragonal crystal takes the form

$$\langle I_B \rangle = K\frac{\langle \Delta z^2 \rangle}{c^{5.5}}\cos^2\theta + K\frac{\langle \Delta r_{\perp}^2 \rangle}{2a^{5.5}}\sin^2\theta \tag{8}$$

where $\langle \Delta z^2 \rangle$ is the mean-square displacement (MSD) of the Ti atom along the $z$-axis from the centre of the $[O_1O_2]$ segment which is parallel to this axis, $\langle \Delta r_{\perp}^2 \rangle = \langle \Delta x^2 \rangle + \langle \Delta y^2 \rangle$ is the MSD of the Ti atom in the $x$, $y$ plane from the centre of the coordination polyhedron, $\langle \Delta x^2 \rangle$ and $\langle \Delta y^2 \rangle$ are the corresponding MSDs for the $x$, $y$-axes (of course, in the case of tetragonal symmetry $\langle \Delta x^2 \rangle = \langle \Delta y^2 \rangle$), $c$ and $a$ are the crystal lattice parameters.

It is reasonable to obtain the expression for the peak B area in the case of the polycrystal sample. Such an expression can be easily obtained from equation (8) if one takes into account that after averaging over all possible orientations of the crystallites in the polycrystal sample the following equations take place, $\langle \cos^2\theta \rangle = 1/3$, $\langle \sin^2\theta \rangle = 2/3$. Then one has

$$\langle I_B \rangle = \frac{K}{3} \cdot \left( \frac{\langle \Delta z^2 \rangle}{c^{5.5}} + \frac{\langle \Delta r_{\perp}^2 \rangle}{a^{5.5}} \right). \tag{9}$$

In the case of the cubic crystal $\langle \Delta z^2 \rangle = \langle \Delta x^2 \rangle = \langle \Delta y^2 \rangle$ and $c = a$. Hence, the following equation takes place for the averaged peak B area in this case

$$\langle I_B \rangle = K\frac{\langle \Delta r^2 \rangle}{3c^{5.5}} \tag{10}$$

where $\langle \Delta r^2 \rangle = 3\langle \Delta z^2 \rangle$ is the MSD of the Ti atom from the centre of the coordination polyhedron for the cubic crystal.

Taking into account that distortion of the ideal perovskite-structure cubic lattice is relatively weak for all perovskite-structure crystals, the last equation obtained for cubic crystals can also be considered an approximate equation which connects the peak B area measured for any perovskite-structure polycrystal sample to the MSD of the Ti atom from the centre of the coordination polyhedron in this crystal. Such a result can easily be derived from equation (9) if one assumes that for all perovskites $a \approx c$.

The second case for which one can obtain a simple expression for the averaged area $\langle I_B \rangle$ occurs if one assumes a model for the atomic structure of the perovskites proposed in [9, 37]. According to this model which is suitable for lead titanate in both tetragonal and cubic phases the interatomic spacings in $TiO_6$ octahedrons do not depend practically on the temperature. Each octahedron is strongly tetragonally distorted and the Ti atom is displaced from the centre of the octahedron along its local four-fold axis $c'$. At low temperature nearly all $c'$-axes are directed along the macroscopic tetragonal axis $z$ of the crystal but an increase of temperature leads to the appearance of octahedrons with local $c'$-axes perpendicular to the macroscopic $z$-axis and parallel to either $x$ or $y$ axes. At high temperature in the cubic phase all three possible directions for the axis $c'$ of each $TiO_6$ octahedron have the same probability, equal to $1/3$. The direction of the $c'$-axis of the definite octahedron is not static, of course. Unfortunately x-ray spectra, which are determined by the positions of atoms, not by their velocities, cannot give information about the dynamic processes in the crystals. Let $w$ be the probability for the $c'$-axis to be directed along the $z$-axis of the crystal and $c$ be the spacing between the oxygen atoms disposed at the local $c'$-axis of the $TiO_6$ octahedron. One can then easily obtain the following equation for the averaged peak B area instead of equation (8)

$$\langle I_B \rangle = K \frac{\Delta z^2}{c^{5.5}} \left( w \cos^2 \theta + \frac{1-w}{2} \sin^2 \theta \right) \tag{11}$$

where $\Delta z$ is the displacement of the Ti atom from the centre of the $TiO_6$ octahedron along the $c'$ direction.

It is worth noting that the results obtained here are also valid for the other perovskite-structure crystals $ABO_3$ where the atom B is the TM atom.

To avoid misunderstandings it is necessary to take into account the following two facts. First, the MSD introduced earlier are formed by both static displacement of the Ti atom from the centre of the coordination polyhedron and by thermal vibrations of the atoms. The partial contributions into the MSD originating from the static and dynamic displacements cannot be distinguished from each other by x-ray absorption spectroscopy. Second, it is necessary to stress that the displacements considered are the displacements of the Ti atom relative to the instantaneous positions of the nearest oxygen atoms but not the displacements of the Ti atom from the centrally-symmetric site in the perovskite structure lattice. So, one cannot consider that the large value of the MSD $\langle \Delta r^2 \rangle$ estimated from the experimental PEFS [9] for cubic lead titanate means that the amplitudes of Ti atom thermal vibrations in the cubic lattice are dramatically large. On the contrary, it is quite possible that such a large value of the MSD is caused by large displacements of oxygen atoms from the sites in the direction of the nearest Ti atoms. The diffraction data in [38], which indeed confirm the anomalous large amplitudes of thermal vibrations of the oxygen atoms in these directions, indicate the last possibility to be the most probable in the case of cubic lead titanate.

We would like also to stress that the peak B area is proportional to the TM atom MSD which is essentially determined by the three-particle atomic distribution function. Consequently, information about the atomic structure of a crystal which is available from the PEFS cannot be obtained, in principle, by diffraction methods or by the EXAFS. As a result the PEFS data are very important for studies of the microscopic mechanisms of the

crystal lattice reconstruction during the phase transitions in the TM oxides. For instance, comparing EXAFS and PEFS data one is able to obtain information about the three-particle correlations in the crystal.

### *3.3. The effect of 4d atom presence in the vicinity of the absorbing 3d atom in solid solutions on the PEFS*

The experimental Ti-K XAS PEFS obtained in [10] for a row of solid solutions $PbTi_xZr_{1-x}O_3$ (so-called PZT) with atomic concentrations of Ti atoms $x = 0.52$ (middle curve) and $x = 0.3$ (lower curve) are presented in figure 7. It is evident from this picture that the presence of Zr atoms in PZT leads to the appearance of an additional high-energy peak C′ in the Ti K-XAS PEFS whose intensity increases with Zr atom concentration whereas the intensity of peak C simultaneously decreases. This phenomenon could be easily understood if one takes into account that the energy of the Zr 4d shell exceeds that of the Ti 3d shell by about 3 eV [13]. Hence, the peak C′ is caused most probably by the transitions of the Ti 1s electrons into the $e_g$ MO of the neighbouring $ZrO_6$ octahedrons. To confirm such an assumption we have calculated the Ti K-XANESs for the 51-atomic clusters which contain, within the six oxygen octahedrons surrounding the central absorbing Ti atom, two (figure 8, curve 2) and four (figure 8, curve 3) Zr atoms. One can see that the calculated spectra presented in figure 8 are in reasonable agreement with the experimental ones thus confirming the interpretation proposed.

One can expect that the areas of the peaks C and C′ can provide direct information about the average number of 4d TM atoms in the oxygen octahedrons surrounding those

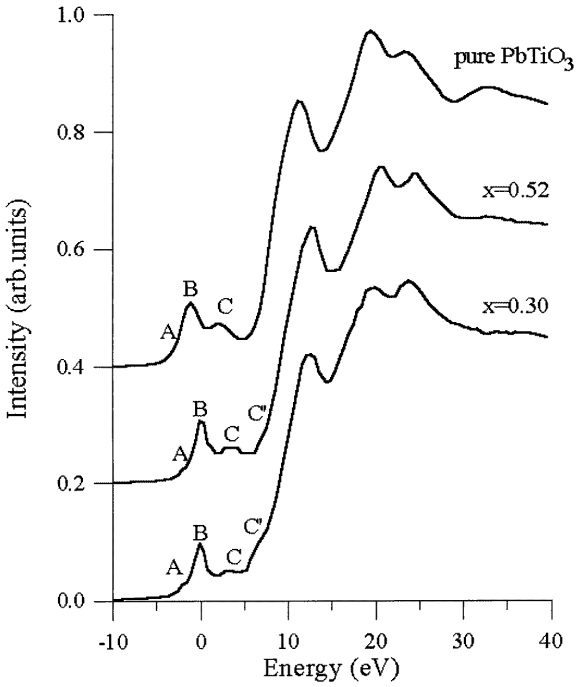


**Figure 7.** The experimental Ti K-XANES [10] for the $PbTiO_3$ polycrystal (upper curve) and for the solid solutions $PbTi_xZr_{1-x}O_3$ (PZT) for: $x = 0.52$ (middle curve) and $x = 0.3$ (lower curve).

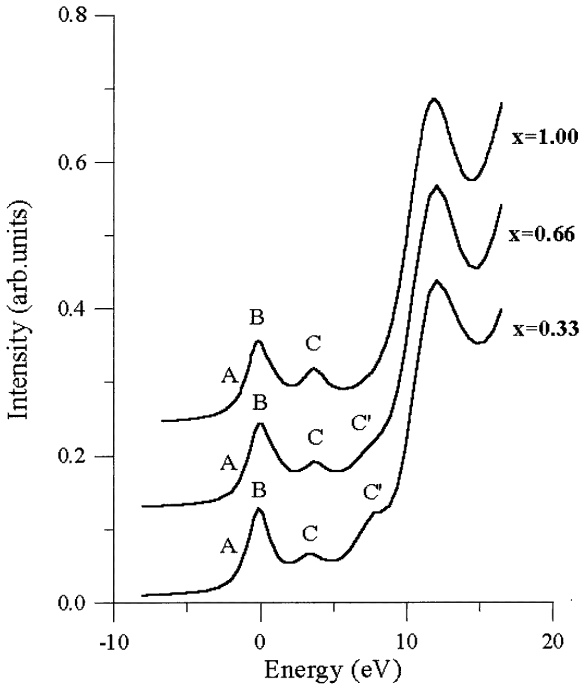


**Figure 8.** The calculated Ti K-XANES for the $PbTiO_3$ polycrystal (upper curve) and for the solid solutions $PbTi_xZr_{1-x}O_3$ (PZT) for: $x = 0.66$ (middle curve) and $x = 0.33$ (lower curve).

containing 3d atoms thus allowing us to study the correlations in the ion distribution in the solid solutions.

## 4. Conclusion

The calculation method proposed in the present paper has been confirmed by a successful comparison of theoretical Ti K-XANESs for the perovskite-structure titanates $PbTiO_3$ and $EuTiO_3$ with experiment. Numerous calculations have been carried out by this method for various perovskite-structure clusters. The results of such computer experiments have enabled us to ascertain the nature of all the peaks in the pre-edge fine structure (PEFS) of the x-ray absorption spectra investigated. In order to do this we compared: (i) the Ti K-PEFS with Ti d-LDOS in both ground and excited states, (ii) the Ti K-PEFS calculated for different values of the atomic potential shifts in the MT spheres of the absorbing Ti atom and neighbouring Ti atoms, (iii) the Ti K-PEFS calculated for different positions of the absorbing Ti atom in the coordination polyhedron, in particular, for the Ti atom placed into the centre of this polyhedron.

Employing the results obtained we have shown that the low-intensity long-wave side peaks A in the PEFSs considered are caused mainly by quadrupole transitions of Ti 1s electrons to 3d-originated unoccupied $t_{2g}$-type MO of the absorbing $TiO_6$ polyhedron affected by the screened 1s-hole potential. The peaks B which are observed at about 3 eV above peaks A are proved to be caused by the Ti 1s electron transitions to the absorbing $TiO_6$ polyhedron 3d-originated unoccupied p–d hybrid orbitals of $e_g$-type symmetry which are also affected by the 1s-hole potential. Hybridization (p–d mixture effect) takes place owing to the static and/or dynamic violation of the inversion symmetry relative to the absorbing Ti atom.

The area of peak B strongly depends on the displacement of the absorbing Ti atom from the instantaneous centre of the Ti atom coordination polyhedron and on the x-ray polarization vector direction. Such dependence can be successfully employed for the quantitative determinations of the Ti atom displacements but even qualitative analysis of the PEFSs in experimental Ti K-XAS for perovskite-structure titanates provides interesting results. Namely, comparing the experimental Ti K-XAS for the $PbTiO_3$, $BaTiO_3$, $SrTiO_3$, $CaTiO_3$, and $EuTiO_3$ polycrystals shown in figure 1 and PZT ceramics shown in figure 7 one can see that the intensive peaks B only appear for the ferroelectric crystals $PbTiO_3$, $BaTiO_3$, and PZT both below and above the Curie point whereas in para-electric crystals $SrTiO_3$, $CaTiO_3$, and $EuTiO_3$ the peaks B are very weak. One can consider consequently the intensive peak B in the Ti K-XAS to be a qualitative spectroscopic indication for ferroelectricity in perovskite-structure titanates. The features of the crystal lattice dynamics which cause the intensive peak B in the cubic phase above the Curie point should be a subject for further investigations. Comparison of the data obtained from the PEFS and EXAFS analysis and also from x-ray and neutron diffraction should provide new information about lattice dynamics and the mechanisms of phase transitions in the crystals considered. It is worth noting that the peak B area is essentially determined by the three-particle atomic distribution function.

The short-wave side peaks C which appear above the peaks B by about 3 eV are shown to be caused by Ti 1s electron transitions to the unoccupied 3d-originated $e_g$-type MO of $TiO_6$ polyhedra neighbouring the absorbing Ti atom which are weakly affected by the core hole potential. The peak C area does not depend strongly on small displacements of the atoms from their sites in a cubic crystal lattice but it changes significantly when 4d atoms appear in the vicinity of the absorbing Ti atom (for instance, Zr atoms in PZT solid solutions). In such a case an additional peak C′ appears which is shifted to the short-wave side direction from peak C by about 3 eV. This peak is caused by Ti 1s electron transitions to the unoccupied 4d-originated $e_g$-type MO of the neighbouring polyhedra containing 4d atoms. The peak C′ area is directly determined by the average number of 4d atoms in the nearest vicinity of the absorbing Ti atom. The peaks C and C′ can be successively employed for studies of the distribution of 4d atoms around 3d ones in perovskite-structure solid solutions.

## Acknowledgments

The authors are grateful to Professor E A Stern and Dr B Ravel for useful discussions and for the experimental spectra. The work has been supported by the Russian Foundation for Basic Research (grant Nos 95-02-05828a and 97-02-17215).

## References

[1] Balzarotti A, Comin F, Incoccia L, Piacentini M, Mobilio S and Savoia A 1980 *Solid State Commun.* **35** 145
[2] Grunes L A 1983 *Phys. Rev.* B **27** 2111
[3] Dräger G, Frahm R, Materlik G and Brummer O 1988 *Phys. Status Solidi* b **146** 287
[4] Kraizman V L, Novakovich A A, Popov V I, Cherkashenko V M and Kurmaev E Z 1990 *Ukrain. Fiz. Dz.* **35** 915
[5] Poumellec B, Cortes R, Loisy E and Berthon J 1994 *Phys. Status Solidi* **103** 335
[6] Waychunas G A, Apted J and Brown G Jr 1983 *Phys. Chem. Minerals* **10** 1
[7] Manceau A, Gorshkov A I and Drits V A 1992 *Am. Mineral.* **77** 1133
[8] Bajt S, Sutton S R and Delaney J S 1994 *Geochim. Cosmo. Acta* **58** 5209
[9] Ravel B, Stern E A, Yacobi Y and Dogan F 1993 *Japan. J. Appl. Phys. Suppl.* **32**-2 782
[10] Ravel B and Stern E A 1995 *Physica* B **208/209** 316
[11] Vedrinskii R V, Kraizman V L, Novakovich A A, Urazhdin S V, Demekhin Ph V, Ravel B and Stern E A 1997 *J. Physique* IV **7** 107
[12] Mattheiss L F 1972 *Phys. Rev.* B **6** 4718

[13] Harrison W A 1980 *Electron Structure and the Properties of Solids* (San Francisco, CA: Freeman)
[14] Leapman R D and Grunes L A 1980 *Phys. Rev. Lett.* **45** 397
[15] Leapman R D, Grunes L A and Fejes P J 1982 *Phys. Rev.* B **26** 614
[16] Bianconi A 1982 *Phys. Rev.* B **26** 2741
[17] Crocombette J P and Jollet F 1994 *J. Phys.: Condens. Matter* **6** 10 811
[18] Poumellec B, Marucco J F and Touzelin B 1987 *Phys. Rev.* B **35** 2284
Poumellec B, Durham P J and Guo G Y 1991 *J. Phys.: Condens. Matter* **3** 8195
[19] Khan M A, Kotani A and Parlebas J C 1991 *J. Phys.: Condens. Matter* **3** 1763
Brydson R, Sauer H, Engel W, Thomas J M, Zeitler E, Kosugi N and Kuroda H 1989 *J. Phys.: Condens. Matter* **1** 797
[20] Uozumi T, Okada K, Kotani A, Durmeyer O, Kappler J P, Beaurepaire E and Parlebas J C 1992 *Europhys. Lett.* **18** 85
[21] Wu Z Y, Ouvrard G, Gressier P and Natoli C R 1997 *Phys. Rev.* B **55** 10 382
[22] Heitler W 1936 *The Quantum Theory of Radiation* (Oxford: Clarendon)
[23] Johnson K H and Smith F C 1972 *Phys. Rev.* B **5** 831
[24] Vedrinskii R V and Novakovich A A 1975 *Fis. Metall. Metallovedenie* **39** 7
[25] Ashley C A and Doniach S 1975 *Phys. Rev.* B **11** 1279
[26] Nemoshkalenko V V and Timoshevskii A N 1985 *Phys. Status Solidi* b **127** 163
[27] Doniach S, Berding M, Smith T and Hodgson K O 1984 *EXAFS and Near Edge Structure III* ed K O Hodgson, B Hedman and J E Penner-Hahn (Berlin: Springer) p 33
[28] Herman F and Skillman S 1963 *Atomic Structure Calculation* (Englewood Cliffs, NJ: Prentice-Hall)
[29] Schwarz K 1972 *Phys. Rev.* B **5** 2466
[30] Bugaev L A, Gegusin I I, Datsyuk V N, Novakovich A A and Vedrinskii R V 1986 *Phys. Status Solidi* b **133** 192
[31] Shirane G and Pepinsky R 1955 *Phys. Rev.* **97** 1179
[32] Holzapfel H and Sieler J 1966 *Z. Anordan. Allgem. Chem.* **343** 174
[33] Bell M I, Elam K H and Elam W T 1991 *Ferroelectrics* **120** 103
[34] Aifa Y, Poumellec B, Jeanne-Rose V, Cortes R, Vedrinskii R V and Kraizman V L 1997 *J. Physique* IV **7** 217
[35] Kraizman V L, Novakovich A A, Vedrinskii R V and Timoshevskii V A 1995 *Physica* B **208/209** 35
[36] Aifa Y, Poumellec B, Cortes R, Vedrinskii R V, Kraizman V L and Demekhin Ph V 1997 *J. Physique* IV **7** 219
[37] Ravel B and Stern E A 1997 *J. Physique* IV **7** 1223
[38] Glazer A M and Mabud S A 1978 *Acta Crystallogr.* B **34** 1065